

Deep Magnification-Arbitrary Upsampling over 3D Point Clouds

Yue Qian, Junhui Hou, *Senior Member, IEEE*, Sam Kwong, *Fellow, IEEE*, and Ying He, *Member, IEEE*

Abstract—This paper addresses the problem of generating dense point clouds from given sparse point clouds to model the underlying geometric structures of objects/scenes. To tackle this challenging issue, we propose a novel end-to-end learning based framework, namely MAPU-Net. Specifically, by taking advantage of the linear approximation theorem, we first formulate the problem explicitly, which boils down to determining the interpolation weights and high-order approximation errors. Then, we design a *lightweight* neural network to adaptively learn unified and sorted interpolation weights and normal-guided displacements, by analyzing the local geometry of the input point cloud. MAPU-Net can be interpreted by the explicit formulation, and thus is more memory-efficient than existing ones. In sharp contrast to the existing methods that work only for a pre-defined and fixed upsampling factor, MAPU-Net, a single neural network with one-time training, can handle an arbitrary upsampling factor, which is highly desired in real-world applications. In addition, we propose a simple yet effective training strategy to drive such a flexible ability. Extensive experiments on both synthetic and real world data demonstrate the superiority of the proposed MAPU-Net over state-of-the-art methods both quantitatively and qualitatively. To the best of our knowledge, this is the first end-to-end learning based method that is capable of achieving magnification-arbitrary upsampling over 3D point clouds.

Index Terms—Point cloud, sampling, linear approximation, deep learning, surface reconstruction.

I. INTRODUCTION

OWING to the flexibility and efficiency in representing objects/scenes of complex geometry and topology, point clouds are widely used in immersive telepresence [29], 3D city reconstruction [20], [27], cultural heritage reconstruction [44], [4], geophysical information systems [30], [28], autonomous driving [5], [22], and virtual/augmented reality [12], [37]. Despite of great progress of 3D sensing technology [11], [18] in recent years, it is still costly and time-consuming to acquire dense point clouds for representing shapes with rich geometric details, which are highly desired in downstream applications. Instead of relying on hardware improvement, we are interested in developing a computational method that is able to upsample a given sparse, low-resolution point cloud to a dense one that faithfully represents the underlying surface (see Fig. 1). Since the upsampling problem is often thought

as a 3D counterpart of image super-resolution [21], [49], intuitively one may consider borrowing powerful techniques from image processing community. However, due to the unordered and irregular nature of point clouds, such an extension is far from trivial, especially when the underlying surface has complex geometry and/or topology. Besides, the two types of data are essentially different i.e., 3D point clouds represent explicit geometry information of objects/scenes, while 2D images only record the reflected light intensities (i.e., color) by objects/scenes, which hinders the straightforward extension of well-developed image super-resolution techniques to some extent.

There are roughly two categories of methods for point cloud upsampling: optimization-based methods [3], [25], [15], [31], [16], [43] and deep learning based methods [48], [47], [42] and [23]. The former usually fits local geometry and works well for smooth surfaces with less features. However, these methods struggle with multi-scale structure preservation. The latter adopts trained neural networks to adaptively learn structures from data, and outperforms optimization based methods to a significant extent. However, the existing deep learning based methods take little consideration of the geometric properties of 3D point clouds, which limits their performance. Moreover, they were designed for a *fixed* upsampling factor. To handle upsampling with varying factors, one has to build multiple networks and train each of them with a pre-defined factor, which increases both the model complexity and the training time significantly. Thus, a single network that is trained only once and can support an arbitrary upsampling factor is highly desired in real-world applications.

In this paper, based on the linear approximation theorem, we propose MAPU-Net, a novel end-to-end learning based magnification-arbitrary upsampling method for 3D point clouds, which is capable of upsampling an input point cloud with an arbitrary factor after one-time training. Technically, given a query point \mathbf{x}_i , MAPU-Net first creates new points in its local neighborhood as the affine combination of its neighboring points, where unified and sorted interpolation weights are adaptively learned by analyzing the local geometry structure, instead of being predefined. These newly generated points are distributed in the convex hull of the neighbouring points. Then MAPU-Net refines the coordinates of the coarse points along the normal direction of \mathbf{x}_i , which is also achieved in a data-driven manner. Besides, we propose a simple yet effective training strategy to drive the learning of the flexibility of our network. Through extensive experiments and evaluations on both synthetic and real world data, we demonstrate that the proposed MAPU-Net, a single network

This work was supported in part by the Natural Science Foundation of China under Grants 61871342, and in part by the Hong Kong Research Grants Council under grants 9042955 (CityU 11202320) and 9042955 (CityU 11202320) (*Corresponding Author: Junhui Hou*)

Y. Qian, J. Hou, and S. Kwong are with the Department of Computer Science, City University of Hong Kong, Hong Kong. Email: yueqian4-c@my.cityu.edu.hk; jh.hou@cityu.edu.hk; cssamk@cityu.edu.hk

Y. He is with the School of Computer Science and Engineering, Nanyang Technological University, Singapore, 639798. Email: yhe@ntu.edu.sg

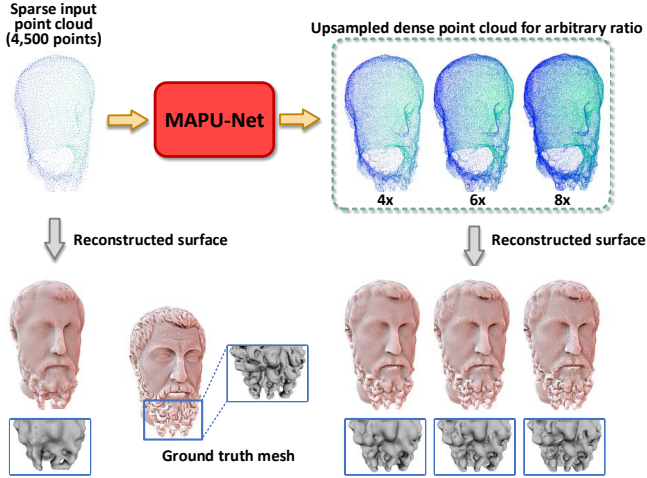


Fig. 1: MAPU-Net can upsample a sparse point cloud with an arbitrary factor not greater than the maximum upsampling factor after one-time training. In this example, the maximum upsampling factor is equal to 8. Here we only show upsampling results for factors $4\times$, $6\times$ and $8\times$, and observe MAPU-Net can generate meaningful geometric details. Moreover, the generated details are richer and closer to the ground truth ones with the factor increasing.

after one-time training, consistently outperforms state-of-the-art methods for upsampling factors from $4\times$ to $16\times$ to a significant extent in terms of four commonly used quantitative metrics. Qualitatively, 3D meshes reconstructed from the densified points of MAPU-Net contain richer geometric details than those of state-of-the-art approaches. More importantly, owing to our unique and explicit formulation towards the 3D point cloud upsampling problem, the proposed MAPU-Net is much more memory-efficient and more interpretable than existing methods.

The rest of this paper is organized as follows. Section II reviews existing methods on point cloud upsampling. Section III formulates the point cloud upsampling problem in an explicit manner by using the linear approximation theorem. Section IV presents the proposed framework, followed by experimental results and comparisons in Section V. Finally, Section VI concludes the paper.

II. RELATED WORK

A. Optimization based Methods

Over the past decade, a number of optimization based methods for point cloud upsampling/resampling have been proposed. For example, Alexa *et al.* [3] upsampled points by referring the Voronoi diagram, which requires the surface smoothness assumption and computes on the moving least squares surface. Based on a locally optimal projection operator (LOP), Lipman *et al.* [25] developed a parametrization-free method for point resampling and surface reconstruction. Subsequently, Huang *et al.* [15] and Preiner *et al.* [31] proposed weighted LOP and continuous LOP, respectively. Specifically, the weighted LOP iteratively consolidates point

clouds by means of normal estimation, and thus is robust to noise and outliers. The continuous LOP can perform fast surface reconstruction by adopting a Gaussian mixture model. However, LOP-based methods assume that points are sampled from smooth surfaces, which degrades upsampling quality towards sharp edges and corners. To effectively preserve the sharp features, Huang *et al.* [16] presented an edge-aware (EAR) approach, which first resamples points away from edges with reference to given normal information, then progressively upsamples points to approach the edge singularities. However, the performance of EAR heavily depends on the given normal information and parameter tuning. By introducing the concept of deep point, Wu [43] proposed a method to jointly perform point cloud completion and consolidation under the guidance of extracted Meso-skeletons. The method can successfully recover regions with holes; however, it is sensitive to noise and outliers. In conclusion, optimization based point cloud upsampling methods either assume insufficient hypotheses or require additional attributes, which limit their performance.

B. Deep Learning based Methods

The great success of deep learning in image/video processing and analysis has been encouraged both academia and industrial to explore the potential of deep learning on 3D point cloud processing and analysis. However, the unordered and irregular characteristics of point clouds make it non-trivial. Qi *et al.* [34] pioneered PointNet, the first deep learning based platform that can directly process the raw 3D point cloud data. The shared MLP per point and the symmetric max-pooling operation help PointNet to cope with the irregular and unordered characteristics of point clouds. Afterwards, there are emerging works striving to extract more meaningful and discriminative features with awareness of local and global information. For example, PointNet++ [35] exploits the local geometry structure by aggregating features of neighbouring points. DGCNN [41] considers dynamic neighbors based on the feature distance. PointCNN [24] permutes order of points in a local region to apply shared convolution for all candidate points. These deep learning based methods have achieved promising results in point cloud classification and segmentation. Moreover, they are also adopted as backbones to extract high dimensional features in other point cloud processing tasks, such as detection [32], [33], [39], registration [26], [40], [46] and reconstruction [2], [7], [45].

Recently, Yu *et al.* [48] proposed the first deep learning algorithm for point cloud upsampling, called PU-Net, which employs PointNet++ to extract point-wise features and the expands the features by multi-branch MLPs. A joint reconstruction and repulsion loss function is adopted to train PU-Net such that generated point clouds are with uniform density. Although PU-Net outperforms the previous optimization based approaches, there is no guarantee that the generated points are uniformly distributed, as it overlooks the spatial relations among the points severely. The follow-up work, namely EC-Net [47], adopts a joint loss of point-to-edge distance to preserve sharp edges. However, EC-Net requires training data with annotated edge and surface information, which is tedious

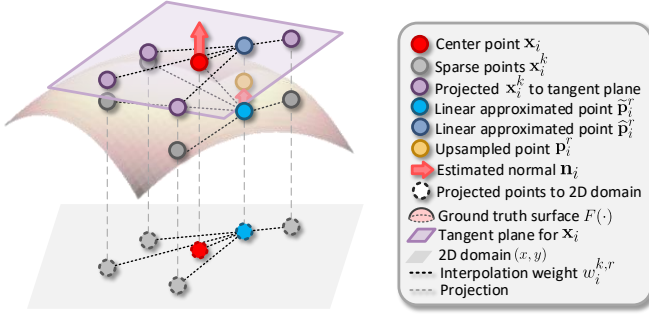


Fig. 2: The local neighborhood of a 3D surface around point \mathbf{x}_i (red) can be approximated by the tangent plane at \mathbf{x}_i . Therefore, the upsampled point \mathbf{p}_i^r can also be approximated by a linear combination of neighboring points projected onto the tangent plane. To avoid calculation of tangent plane, \mathbf{p}_i^r can also be estimated by the linear interpolation directly from sparse neighborhood points.

to obtain in practice. Inspired by the cascaded structure in image super-resolution, Wang *et al.* [42] proposed a patch-based progressive point cloud upsampling method (3PU-Net), which can progressively upsample an input to a relatively large upsampling factor, say $16\times$. Specifically, 3PU-Net replicates the point-wise features and separates them by appending a 1D code $\{-1, 1\}$. However, 3PU-Net does not model the local geometry well. Also, it requires a careful step-by-step training. In addition, the way of appending a 1D code limits each subnet upsamples an input by a factor 2, and thus 3PU-Net only supports the overall upsampling factor in powers of 2. By introducing an additional discriminator, Li *et al.* [23] developed an adversarial framework, called PU-GAN, to boost the quality of upsampled point clouds.

III. PROBLEM FORMULATION

Denote by $\mathcal{X} = \{\mathbf{x}_i | \mathbf{x}_i \in \mathbb{R}^3\}_{i=1}^M$ a sparse point cloud with M points and a user-specified scaling factor R . Our objective is to generate a dense point cloud $\mathcal{P}_R = \{\mathbf{p}_i^r | \mathbf{p}_i^r \in \mathbb{R}^3\}_{i,r=1}^{M,R}$, which contains more geometric details to approximate the underlying surface. Specifically, for each point of \mathcal{X} , we interpolate a certain number of nearest neighboring points located in its neighborhood to generate additional R points.

In order to formulate the problem, we first consider a local neighborhood of point $\mathbf{x}_i = (x_i, y_i, z_i)$ and its K nearest neighboring points $\{\mathbf{x}_i^k = (x_i^k, y_i^k, z_i^k)\}_{k=1}^K$. We assume the surface is locally smooth at \mathbf{x}_i so that it can be represented by a smooth implicit function $f(\cdot)$, i.e.,

$$f(x, y, z) = 0. \quad (1)$$

Therefore, the neighboring points satisfy $f(x_i^k, y_i^k, z_i^k) = 0$. If the partial derivative $\frac{\partial f}{\partial z}$ does not vanish, the local surface can be expressed explicitly as a height function $F: \mathbb{R}^2 \rightarrow \mathbb{R}$ using the implicit function theorem [13], i.e.,

$$z = F(x, y). \quad (2)$$

Using Taylor expansion, we can locally approximate the surface at (x_i, y_i) as

$$z(x, y) = F(x_i, y_i) + \nabla F(x_i, y_i)^\top \cdot (x - x_i, y - y_i) + O((x - x_i, y - y_i)^2). \quad (3)$$

To generate more points $\{\mathbf{p}_i^r = (\hat{x}_i^r, \hat{y}_i^r, \hat{z}_i^r)\}_{r=1}^R$ locating on the surface, we adopt a 3-step strategy.

First, we express the x - and y -coordinates of each new point (which are also the parameters of the parametric function $z(\cdot, \cdot)$) as the affine combination of known points:

$$(\hat{x}_i^r, \hat{y}_i^r) = \sum_{k=1}^K w_i^{k,r} (x_i^k, y_i^k), \quad (4)$$

where the weights $w_i^{k,r}$ are non-negative and satisfy partition of unity

$$\sum_{k=1}^K w_i^{k,r} = 1, \forall r. \quad (5)$$

Second, we define a linear function $H: \mathbb{R}^2 \rightarrow \mathbb{R}$

$$H(x, y) \triangleq F(x_i, y_i) + \nabla F(x_i, y_i)^\top \cdot (x - x_i, y - y_i),$$

as the first-order approximation of $z(x, y)$. Geometrically speaking, $H(x, y)$ represents the tangent plane of $z(x, y)$ at (x_i, y_i) . Therefore, the z -coordinate \hat{z}_i^r can be approximated as

$$\begin{aligned} \hat{z}_i^r &\approx H(\hat{x}_i^r, \hat{y}_i^r) = H\left(\sum_{k=1}^K w_i^{k,r} (x_i^k, y_i^k)\right) \\ &= \sum_{k=1}^K w_i^{k,r} H(x_i^k, y_i^k) \approx \sum_{k=1}^K w_i^{k,r} z_i^k. \end{aligned} \quad (6)$$

Define $\hat{\mathbf{p}}_i^r \triangleq (\hat{x}_i^r, \hat{y}_i^r, \sum_{k=1}^K w_i^{k,r} H(x_i^k, y_i^k))$ and $\tilde{\mathbf{p}}_i^r \triangleq (\hat{x}_i^r, \hat{y}_i^r, \sum_{k=1}^K w_i^{k,r} z_i^k)$. Note that both $\hat{\mathbf{p}}_i^r$ and $\tilde{\mathbf{p}}_i^r$ are *linear approximations* for \mathbf{p}_i^r (see Fig. 2). Since each $H(x_k, y_k)$ is on the tangent plane, the combined point $\hat{\mathbf{p}}_i^r$ is also on the tangent plane. In contrast, $\tilde{\mathbf{p}}_i^r$ is a linear combination of sample points $\{\mathbf{x}_i^k\}$, therefore it is in its convex hull.

Third, as the linear approximation $\hat{\mathbf{p}}_i^r$ requires tangent plane estimation and the projection of neighborhood points which are non-trivial over point clouds, for simplicity we approximate \mathbf{p}_i^r by using $\tilde{\mathbf{p}}_i^r$, i.e. the direct interpolation of \mathbf{x}_k , together with an approximation error $\mathbf{e}_i^r = (\delta x, \delta y, \delta z)$, i.e.,

$$\mathbf{p}_i^r = \tilde{\mathbf{p}}_i^r + \mathbf{e}_i^r. \quad (7)$$

According to the above theoretical formulation, the problem of interpolating a 3D point cloud boils down to determining the interpolation weights and the approximation errors¹.

IV. PROPOSED METHOD

A. Overview

Motivated by the explicit formation in Section III, we propose a novel data-driven framework to realize 3D point cloud upsampling in an end-to-end fashion, in which the interpolation weights and the approximation error in Eq. (7)

¹Note that the accurate number of nearest neighboring points (i.e., K) is not necessary, because the values of the weights have taken this issue into account, i.e., a point is not a neighbor when $w_i^{k,r} = 0$.

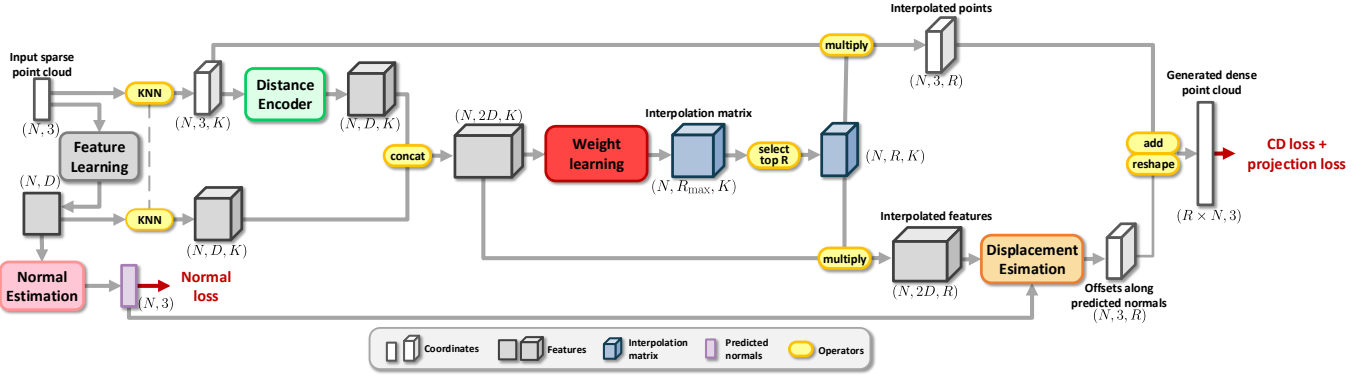


Fig. 3: The flowchart of the proposed MAPU-Net. Given a sparse point cloud with N points, MAPU-Net first learns a D -dimensional feature for each point (i.e., the feature learning module) and also embeds the relative position information of K nearest neighbouring (KNN) points into D -dimensional features (i.e., the distance encoder module). Then the two types of high-dimensional features are concatenated to regress unified and sorted interpolation weights (i.e., the weight learning module), which coarsely interpolate the input sparse point cloud into a dense one. The coarse point cloud is finally refined by learning normal-guided displacements (i.e., the normal estimation module and the displacement estimation module). After one-time end-to-end training, MAPU-Net is capable of handling an arbitrary upsampling factor not greater than the maximum factor R_{max} .

are adaptively learned for each point of \mathcal{X} , by analyzing its local geometry property. As illustrated in Fig. 3, the proposed framework, namely MAPU-Net, is achieved by a *lightweight* neural network, which is mainly composed of three phases, i.e., local feature embedding, learning interpolation weights, and coordinate refinement. Specifically, an input point cloud is first embedded in to a high-dimensional feature space point-by-point via local geometry-aware feature extraction. Then, interpolation weights are learned by regressing the resulting high-dimensional features, which are utilized to interpolate nearest neighbouring points, leading to a coarse upsampled point cloud. Finally, under the guidance of the estimated normals of \mathcal{X} , approximation errors are learned to refine the coordinates of the coarse point cloud. The MAPU-Net is end-to-end trained with a loss function to supervise the the prediction of both coordinates and sparse normals. For an input point cloud with M points, we extract patches containing N points, and MAPU-Net performs upsampling patch by patch.

Note that in contrast to existing deep learning based 3D point cloud upsampling methods that support only a pre-defined and fixed upsampling factor, making them unpractical for real-world applications, the proposed framework is able to achieve magnification-arbitrary upsampling, i.e., it can handle an arbitrary factor after one-time training. Such a flexibility is credited to the unique principle of our framework, which allows us to learn *unified* and sorted interpolation weights. That is, the network is initialized with the maximum factor R_{max} , and the interpolation with a random R ($R \leq R_{max}$) is performed in each iteration during training, i.e., the top- R groups of estimated weights are selected for the $R \times$ upsampling, such that the learned groups of interpolation weights are naturally sorted. Therefore, during inference the top- R groups of estimated interpolation weights could be selected for a specific factor.

In what follows, we will detail the proposed framework

phase by phase.

B. Geometry-aware Local Feature Embedding

In this phase, each 3D point \mathbf{x}_i of \mathcal{X} is projected onto a high-dimensional feature space, denoted by $\mathbf{c}_i \in \mathbb{R}^D$. Particularly, we adopt the dynamic graph CNN (DGCNN) [41] to realize such a process. Unlike previous deep feature representation methods for point clouds [24], [34], [34] which are applied to individual points or a fixed graph constructed with the distance between coordinates, DGCNN defines the local neighborhood based on the distance between features obtained in the preceding layer. Specifically, denote by $\mathcal{E} \subset \mathcal{X} \times \mathcal{X}$ the edges calculated by k -nearest neighbors, then the initial directed graph $\mathcal{G} = (\mathcal{X}, \mathcal{E})$ is updated dynamically from one layer to another layer, based on the feature distance. In addition, it involves dense connections to aggregate multiple levels of features. Though using the local neighborhood in feature space, the learned feature representation \mathbf{c}_i encodes both local and non-local information, while still keeping the permutation invariant property.

Moreover, we adopt a distance encoder [14] to explicitly embed the relative position between points. Such an explicit embedding augments the corresponding point features to be aware of their neighborhood information. Let $\mathcal{S}_i^K = \{\mathbf{x}_i^k\}_{k=1}^K$ be the set of K nearest neighbouring points of \mathbf{x}_i in the sense of the Euclidean distance, and accordingly the associated high-dimensional features of the K points obtained by DGCNN are denoted by $\{\mathbf{c}_i^k\}_{k=1}^K$. The distance encoder employs an MLP to obtain a high-dimensional feature $\mathbf{r}_i^k \in \mathbb{R}^D$ for each neighbouring point, i.e.,

$$\mathbf{r}_i^k = \text{MLP}(\mathbf{x}_i \oplus \mathbf{x}_i^k \oplus (\mathbf{x}_i - \mathbf{x}_i^k) \oplus \|\mathbf{x}_i - \mathbf{x}_i^k\|_2), \quad (8)$$

where \oplus is the concatenation operator, $\|\cdot\|_2$ is the ℓ_2 norm of a vector, and $\text{MLP}(\cdot)$ denotes the MLP process. The encoded

relative distance feature is further concatenated to the feature \mathbf{c}_i^k by DGCNN to form $\tilde{\mathbf{c}}_i^k \in \mathbb{R}^{2D}$:

$$\tilde{\mathbf{c}}_i^k = \mathbf{c}_i^k \oplus \mathbf{r}_i^k. \quad (9)$$

With the explicit encoding of local coordinate information, the high-dimensional feature can capture local geometric patterns.

C. Learning Unified and Sorted Interpolation Weights

As aforementioned, given a upsampling factor R , we aim to generate additional R points for each input point \mathbf{x}_i . As analyzed in Section III, the coarse prediction $\tilde{\mathbf{p}}_i^r$ can be obtained as the affine combination of the K nearest neighboring points, i.e.,

$$\tilde{\mathbf{p}}_i^r = \sum_{k=1}^K w_i^{k,r} \mathbf{x}_i^k$$

$$\text{subject to } \mathbf{x}_i^k \in \mathcal{S}_i^K, \sum_{k=1}^K w_i^{k,r} = 1, \text{ and } w_i^{k,r} \geq 0. \quad (10)$$

To this end, we learn the interpolation weights using a weight learning module, which consists of MLPs applied to the point-wise feature $\tilde{\mathbf{c}}_i^k$. To achieve magnification-arbitrary interpolation, unified and sorted interpolation weights $\mathbb{W}_i^k = [\tilde{w}_i^{k,1}, \tilde{w}_i^{k,2}, \dots, \tilde{w}_i^{k,R_{max}}] \in \mathbb{R}^{R_{max}}$ are learned, i.e., the output size of the weight learning module is initialized to the number of weights for the upsampling with a maximum factor R_{max} , and the learning of such unified weights is modeled as

$$\mathbb{W}_i^k = \text{MLPs}(\tilde{\mathbf{c}}_i^k). \quad (11)$$

Then, for a specific upsampling factor R , the top- R weights of \mathbb{W}_i^k are selected as the corresponding interpolation weights, i.e.,

$$\tilde{\mathbf{w}}_i^k = [\tilde{w}_i^{k,1}, \tilde{w}_i^{k,2}, \dots, \tilde{w}_i^{k,R}] \subseteq \mathbb{W}_i^k. \quad (12)$$

Such a flexible manner is enabled by our unique formulation of the upsampling problem and our special training strategy, i.e., in each iteration of the training process, upsampling with a randomly selected scale factor is performed, and the corresponding weights are updated, so that the learned weights are naturally sorted (see Section IV-E for details).

Moreover, to meet the partition of unity constraint in Eq. (10), we normalize the weights using a softmax layer, i.e.,

$$w_i^{k,r} = \frac{e^{\tilde{w}_i^{k,r}}}{\sum_{k=1}^K e^{\tilde{w}_i^{k,r}}}. \quad (13)$$

As the high-dimensional features explicitly encode relative distance information and local geometry details, it is expected that the weights, which can encourage the interpolated points to fit the underlying surface well, will be predicted.

D. Normal-guided Coordinate Refinement

As formulated in Section III, the generated point $\tilde{\mathbf{p}}_i^r$ via directly interpolating neighbouring points is distributed in the convex hull of the neighbouring points, but not necessary on the underlying curved surface. Therefore, we need an approximation error \mathbf{e}_i^r to compensate the loss. In this subsection,

we adaptively learn such an approximation error to refine the coarse predictions.

Theoretically, the convex hull formed by the k NN points of \mathbf{x}_i and the tangent plane of \mathbf{x}_i are located on the two sides of the surface. On basis of this fact, we can learn a displacement along the normal direction of point \mathbf{x}_i , which promotes point $\tilde{\mathbf{p}}_i^r$ to move towards the underlying surface. First, we propose a normal estimation module, which is capable of predicting the normal of each input point \mathbf{x}_i by regressing its high-dimensional feature \mathbf{c}_i via an identical MLP, i.e.,

$$\mathbf{n}_i = \text{MLP}(\mathbf{c}_i), \quad (14)$$

where $\mathbf{n}_i = (n_x, n_y, n_z)$ is the estimated normal for point \mathbf{x}_i . Then, we apply another MLP to the interpolated high-dimensional feature to regress a displacement δ_i^r , i.e.,

$$\delta_i^r = \text{MLP}\left(\sum_{k=1}^K w_i^{k,r} \tilde{\mathbf{c}}_i^k\right). \quad (15)$$

Finally, the approximation error is derived as

$$\mathbf{e}_i^r = \delta_i^r \mathbf{n}_i = (\delta_i^r n_x, \delta_i^r n_y, \delta_i^r n_z), \quad (16)$$

and the refined point can be obtained as

$$\mathbf{p}_i^r = \tilde{\mathbf{p}}_i^r + \mathbf{e}_i^r. \quad (17)$$

E. Loss Function and Training Strategy

To train the proposed MAPU-Net end-to-end, we design a loss function consisting of the Chamfer distance (CD) loss and a projection distance loss for supervising the upsampled point clouds and a loss for supervising the predicted normals for input sparse point clouds. Let $\mathcal{N} = \{\tilde{\mathbf{n}}_i\}_{i=1}^N$ be the set of normals associated with the points of \mathcal{X} , and $\mathcal{Y}_R = \{\mathbf{y}_l\}_{l=1}^{NR}$ the ground-truth dense point cloud of the $R \times$ upsampling, associated with the normal attribute denoted by $\mathcal{N}_R = \{\bar{\mathbf{n}}_l\}$.

To be specific, the CD loss between the \mathcal{P}_R and \mathcal{Y}_R is defined as

$$L_{cd} = \frac{1}{RN} \left(\sum_{\mathbf{p}_i^r \in \mathcal{P}_R} \|\mathbf{p}_i^r - \phi(\mathbf{p}_i^r)\|_2 + \sum_{\mathbf{y}_l \in \mathcal{Y}_R} \|\mathbf{y}_l - \psi(\mathbf{y}_l)\|_2 \right), \quad (18)$$

where $\phi(\mathbf{p}_i^r) = \arg \min_{\mathbf{y}_l \in \mathcal{Y}_R} \|\mathbf{p}_i^r - \mathbf{y}_l\|_2$, and $\psi(\mathbf{y}_l) = \arg \min_{\mathbf{p}_i^r \in \mathcal{P}_R} \|\mathbf{p}_i^r - \mathbf{y}_l\|_2$. We also introduce the projection distance between upsampled point clouds and ground truth ones, which is defined as

$$L_{pro} = \frac{1}{RN} \sum_{\mathbf{y}_l \in \mathcal{Y}_R} |\bar{\mathbf{n}}_l \cdot (\mathbf{y}_l - \psi(\mathbf{y}_l))|, \quad (19)$$

where $|\cdot|$ returns the absolute value of the input.

To supervise the training of the normal estimation module, we measure the un-oriented difference between the estimated normals and the ground-truth normals:

$$L_{normal} = \sum_{i=1}^N \text{Dist}(\mathbf{n}_i, \tilde{\mathbf{n}}_i), \quad (20)$$

TABLE I: Quantitative comparisons of different methods with various scaling factors. We uniformly scaled the models into a unit cube, so the distance metrics are unitless. Here, we show the average of 13 testing point clouds and mark the best values in bold fonts.

R	Method	Network size	CD (10^{-2})	HD (10^{-2})	JSD (10^{-2})	P2F mean (10^{-3})	P2F std (10^{-3})
4×	EAR [16]	-	0.919	5.414	4.047	3.672	5.592
	PU-Net [48]	10.1 MB	0.658	1.003	0.950	1.532	1.215
	3PU-Net [42]	92.5 MB	0.573	1.073	0.614	0.808	0.809
	PU-GAN-G [23]	7.0 MB	0.660	3.980	1.267	1.605	2.072
	MAPU-Net	4.4 MB	0.562	1.114	0.488	0.582	0.659
8×	EAR [16]	-	-	-	-	-	-
	PU-Net [48]	14.9 MB	0.549	1.314	1.087	1.822	1.427
	3PU-Net [42]	92.5 MB	0.447	1.222	0.511	0.956	0.972
	PU-GAN-G [23]	8.7 MB	0.439	1.673	0.489	0.896	0.846
	MAPU-Net	4.4 MB	0.418	1.136	0.347	0.606	0.705
12×	EAR [16]	-	-	-	-	-	-
	PU-Net [48]	19.7 MB	0.434	0.960	0.663	1.298	1.139
	3PU-Net [42]	-	-	-	-	-	-
	PU-GAN-G [23]	10.3 MB	0.387	2.304	0.442	0.955	0.913
	MAPU-Net	4.4 MB	0.355	1.145	0.313	0.610	0.709
16×	EAR [16]	-	-	-	-	-	-
	PU-Net [48]	24.5 MB	0.482	1.457	1.165	2.092	1.659
	3PU-Net [42]	92.5 MB	0.344	1.355	0.478	0.926	1.029
	PU-GAN-G [23]	11.9 MB	0.351	1.879	0.465	0.941	0.865
	MAPU-Net	4.4 MB	0.318	1.334	0.310	0.614	0.720

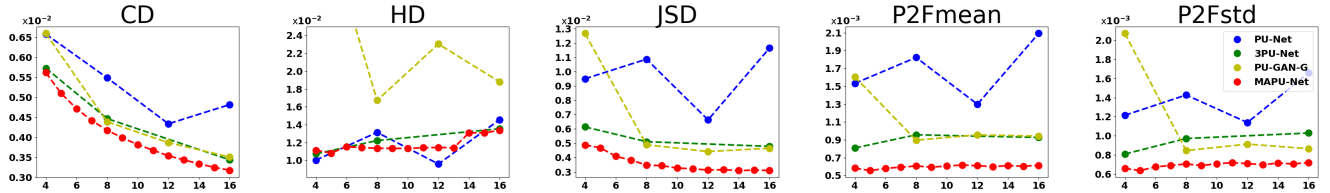


Fig. 4: Illustration of the performance of MAPU-Net with an arbitrary upsampling factor between 4 and 16. The performance of other methods with several feasible factors is shown for reference.

where \mathbf{n}_i is the predicted normal of point \mathbf{x}_i and $\text{Dist}(\mathbf{n}_i, \tilde{\mathbf{n}}_i) \triangleq \min \{ \|\mathbf{n}_i - \tilde{\mathbf{n}}_i\|_2, \|\mathbf{n}_i + \tilde{\mathbf{n}}_i\|_2 \}$.

We define the overall loss function for training MAPU-Net for upsampling with a fixed factor R as

$$L^R = \alpha L_{cd} + \beta L_{pro} + \gamma L_{normal}, \quad (21)$$

where α , β , and γ are three positive parameters. Note that we do not require the ground-truth normals for both sparse and dense point clouds during testing. Our goal is to train a *flexible* MAPU-Net, i.e., after one-time training, MAPU-Net is able to deal with an arbitrary scaling factor during inference. A naive way is to use the summation of the loss function in Eq. (21) for various factors as the loss function, i.e., $L = \sum_j \lambda_j L^{R_j}$ where $\lambda_j > 0$ is the weight to balance different factors. However, it is difficult to tune the parameters λ_j . In our implementation, we randomly select a factor to optimize in each iteration of the training process. Experimental results demonstrate the effectiveness and efficiency of such a simple strategy.

V. EXPERIMENTAL RESULTS

A. Experiment Settings and Implementation Details

Same as previous works [42], [36], we randomly selected 90 high-resolution 3D mesh models from Sketchfab [1] to construct the training dataset and 13 for testing. Applying

Poisson disk sampling [6] to each mesh model, we generated a sparse point cloud with 5K points, and various ground truth dense point clouds for different factors. All points are associated with normals. We then cropped an input point cloud into patches of $N = 256$ points via farthest point sampling [9]. Finally, we applied data augmentation techniques, including random scaling, rotation and point perturbation, to increase data diversity.

We empirically set the coefficients of the loss function in Eq. (21) $\alpha = 20$, $\beta = 20$, and $\gamma = 1$, the parameter $K = 32$ in k-NN, and the maximal upsampling factor $R_{max} = 16$. We used the Adam optimizer [19] with the learning rate 0.001. In each iteration of the training process, we selected the upsampling factor R from 4, 8, 12, and 16 respectively with the probability 0.1, 0.2, 0.3, and 0.4. Note that upsampling with an arbitrary R between 4 and 16 can be conducted during inference. We trained the network with the mini-batch of size 8 for 800 epochs. We implemented MAPU-Net in TensorFlow, and will release the code and trained models.

We employed four commonly used metrics, i.e., Chamfer distance (CD), Hausdorff distance (HD), point-to-surface distance (P2F), and Jensen-Shannon divergence (JSD), to evaluate different methods quantitatively. The P2F distance measures the difference between the upsampled point clouds and the corresponding ground truth 3D mesh models, while the other three metrics evaluate the difference between the upsampled

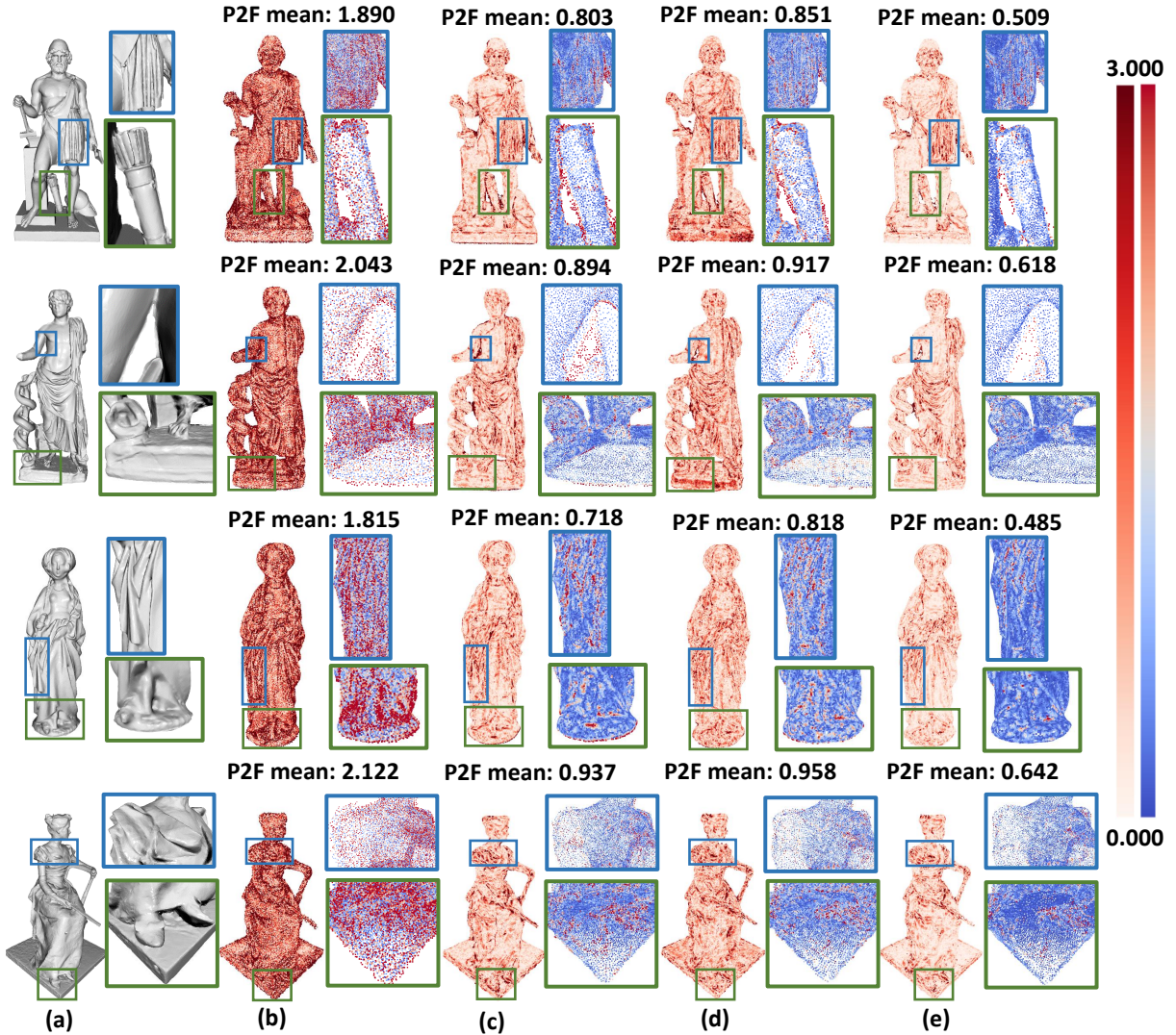


Fig. 5: Comparisons in terms of P2F errors for upsampling factor $R = 16$. We visualized the errors using colors. The left color-bar corresponds to the whole models, while the right one to the closed-up regions. (a) Ground truth mesh models; $16\times$ upsampled point clouds by PU-Net (b), 3PU-Net (c), PU-GAN-G (d) and MAPU-Net (e).

point clouds and the corresponding ground truth dense point clouds. We performed these metrics on a whole point cloud for all compared methods. For all the metrics, the lower the value, the better the quality.

B. Comparison with State-of-the-Art Methods

To demonstrate the advantages of the proposed MAPU-Net, we compared it with optimization based EAR [16] and three state-of-the-art deep learning based methods, i.e., PU-Net [48], 3PU-Net [42] and PU-GAN [23]. Due to large memory consumption, EAR cannot perform tasks with R greater than 4. With the cascaded architecture, 3PU-Net can work only for upsampling factors R in the powers of 2. As PU-GAN is a generative adversarial framework, we used only its generator for fair comparisons, which is denoted as PU-GAN-G. We retrained PU-Net, 3PU-Net and PU-GAN-G on the same dataset and with the same data augmentations as ours. As PU-Net and PU-GAN-G only support upsampling with a

single factor, we trained one network for each upsampling factor.

1) *Quantitative comparison:* Table I shows the average results of 13 testing point clouds, where it can be seen that MAPU-Net can achieve the best performance almost for all upsampling factors in terms of all the four metrics. Besides, it is worth noting that a single MAPU-Net is able to deal with all the upsampling factors, whereas PU-Net and PU-GAN-G require individual networks for each factor. Although 3PU-Net is also a unified model, it can only deal with upsampling factors in powers of 2.

To evaluate the memory-efficiency of different deep learning based methods, we compared their network sizes in Table I, where it can be observed that MAPU-Net has the smallest network size. Due to the progressive upsampling manner, the network size of 3PU-Net, which always produces the second or third best performance, is 21 times as much as ours. PU-Net suffers from the linearly increasing network size since it adopts

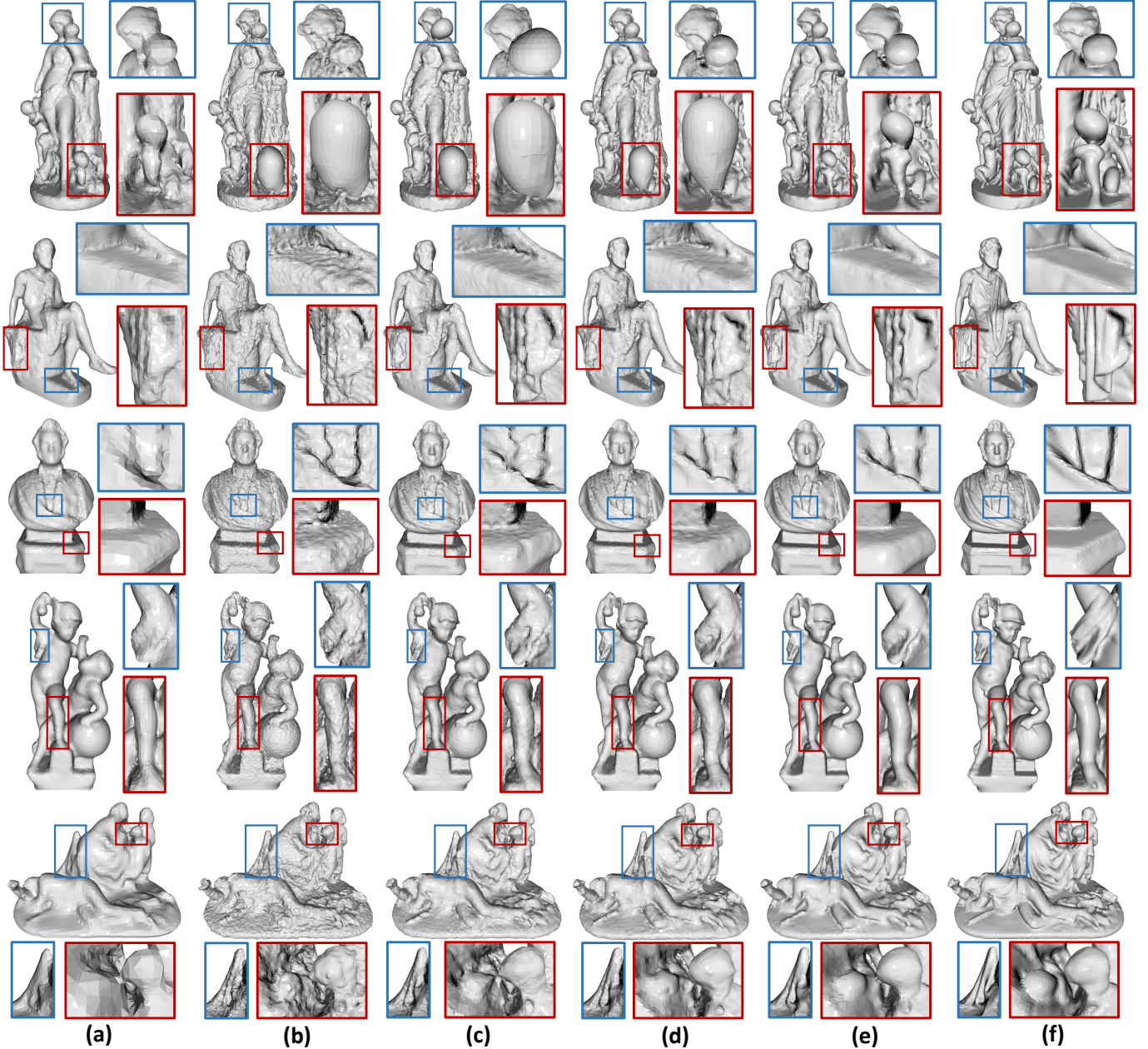


Fig. 6: Visual comparisons of the surfaces reconstructed from (a) sparse point clouds with 5,000 points, the $8\times$ upsampled point clouds by (b) PU-Net, (c) 3PU-Net, (d) PU-GAN-G, and (e) MAPU-Net, and (f) the ground truth dense point clouds with 40,000 points.

the independent multi-branch design for feature expansion.

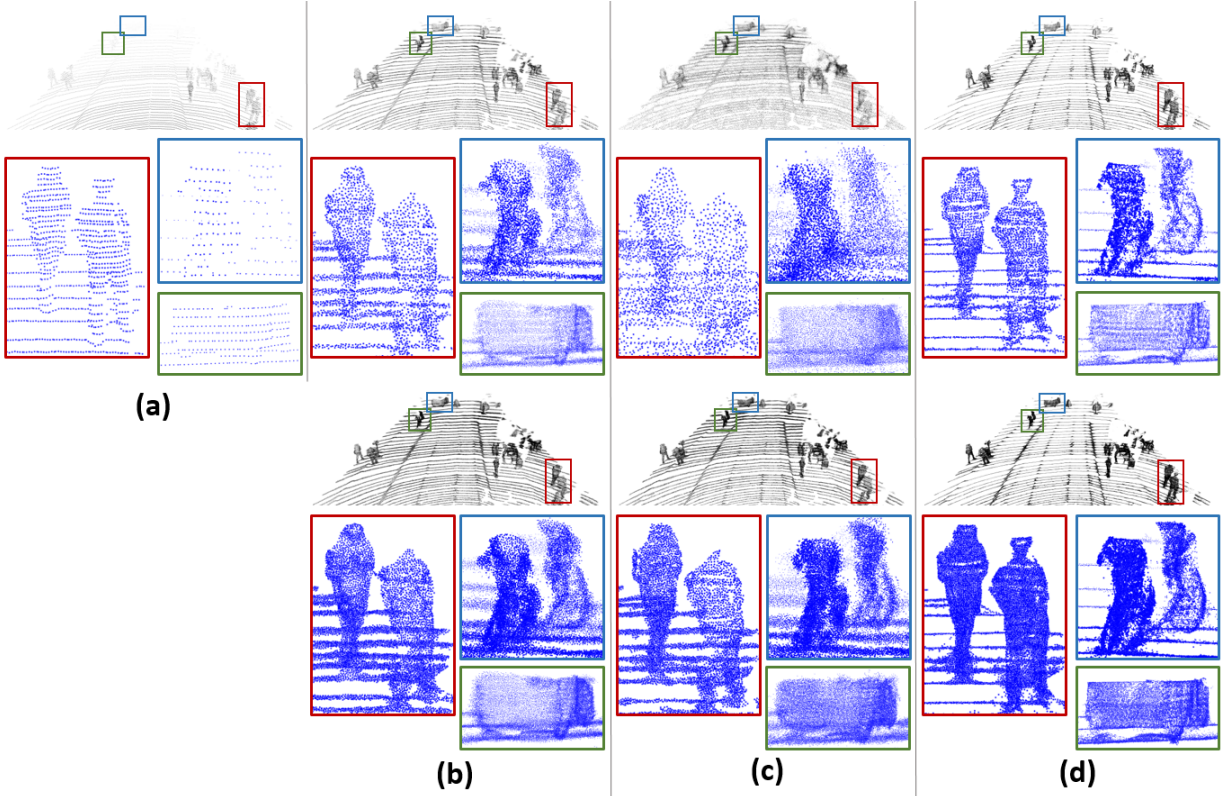
Fig. 4 illustrates the quantitative performance of the proposed MAPU-Net for upsampling with all the factors between 4 and 16. Note that we used only factors 4, 8, 12, and 16 during training. Also, the performance of compared methods with their feasible factors are provided for reference. From Fig. 4, it can be observed that the values of metrics form *smooth* lines with the factor varying (i.e., the red lines), and such a smoothness observation validates the effectiveness of the flexibility of MAPU-Net. Specifically, as the upsampling factor increases, the values of CD and JSD consistently decrease because these two metrics evaluate the distribution difference

between upsampled point clouds and corresponding ground truth dense point clouds, and a larger factor means more generated points, mitigating the overall distribution difference. However, the value of HD increases at relatively large factors, e.g., $R = 14, 15,$ and 16 . The reason is that the HD measures the maximum difference between two point clouds, and a larger factor means a more difficult task (i.e., the ground truth dense point clouds used for evaluation will contain more geometry details, which pose greater challenges), resulting in more distortion.

2) *Visual comparison*: First, we visualized the point-wise P2F errors between the $16\times$ upsampled point clouds by

TABLE II: Ablation studies towards the effectiveness of several key modules contained in MAPU-Net. Here $R = 12$.

Distance encoder	Offset refinement	Normal regression	L_{pro}	CD (10^{-2})	HD (10^{-2})	JSD (10^{-2})	P2F mean (10^{-3})	P2F std (10^{-3})
\times				0.356	1.214	0.324	0.641	0.739
	\times			0.361	1.721	0.402	0.641	0.739
		\times		0.358	1.317	0.336	0.666	0.763
			\times	0.362	1.440	0.320	0.711	0.851
MAPU-Net				0.355	1.145	0.313	0.610	0.709

Fig. 7: Comparisons on real-world LiDAR data. The top and bottom rows are the results of $R = 4$ and 8, respectively. (a) the input sparse point cloud; the results of 3PU-Net (b), PU-GAN-G (c), and MAPU-Net (d).

different methods and corresponding ground truth 3D mesh models in Fig. 5. We observed that the proposed MAPU-Net produces the smallest errors among all methods under comparison. Particularly, MAPU-Net is able to preserve the smoothness for smooth regions better, which is credited to the linear interpolation. In the meantime, MAPU-Net can generate sharper and more detailed areas, thanks to the refinement module.

Second, we demonstrated the effectiveness of MAPU-Net by surface reconstruction in Fig. 6. Specifically, we reconstructed surfaces from the $8\times$ densified point clouds by different methods using Screened Poisson Sampling Reconstruction (SPSR) [17], where point normals were computed by PCA with a neighborhood of 16 points. The identical parameters of SPSR were applied to all point clouds for fair comparisons. From Fig. 6, it can be observed that the surfaces directly reconstructed from the input sparse point clouds are deficient, while those from the upsampled point clouds exhibit richer geometry details. Compared with other methods, the reconstructed surfaces by MAPU-Net are closer to the ground

truth surfaces. Especially, MAPU-Net can recover more details and better preserve the smoothness of smooth regions (see the closed-up regions), which are consistent with the observations from Fig. 5.

C. Evaluation on Real-World Data

We also examined the performance of MAPU-Net on real world point cloud data i.e., one street scene from KITTI [10] captured by LiDAR for autonomous driving, two voxelized full human bodies from the 8iVFB dataset [8] for immersive communication, which were captured via a typical multi-view technique and voxelization, and one building point cloud by fusing the outputs of multiple LiDAR sensors [38].

As shown in Fig. 7, due to the cost of hardware, the original point cloud by LiDAR suffers from sparsity and non-uniformity issues, e.g., objects located in the closed-up regions, including pedestrian, cyclist, and vehicle, are represented with only a few points. The upsampled point clouds by different methods show more geometry details of objects in comparison with the original one. Moreover, com-

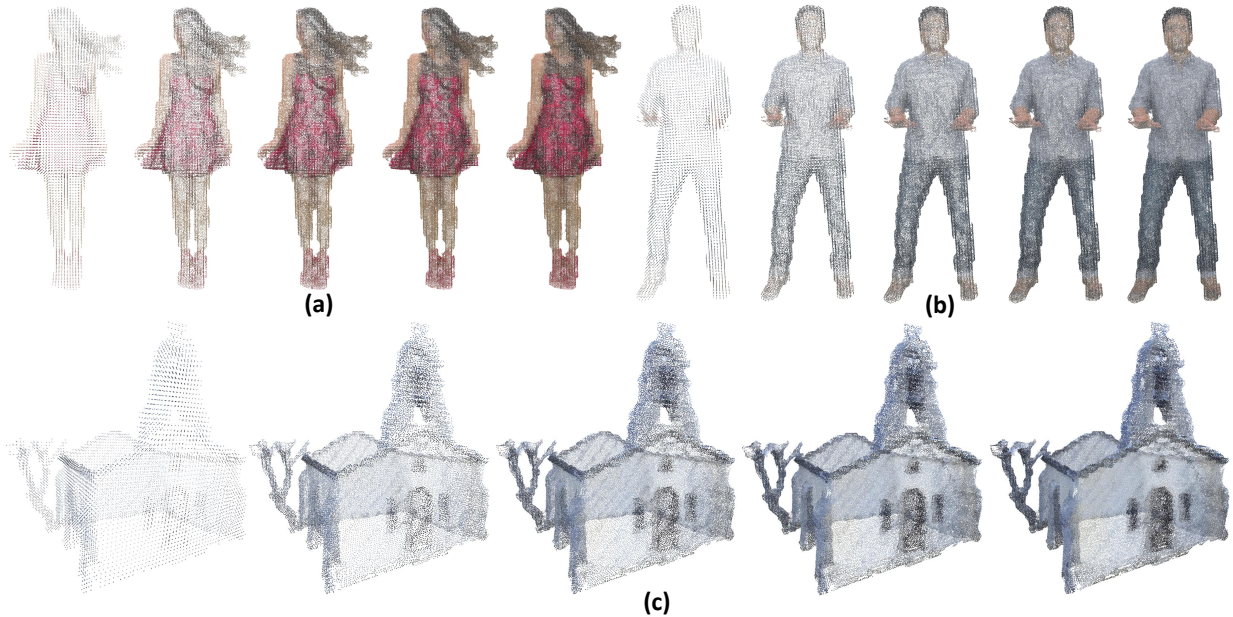


Fig. 8: Results on real-world data with factors $R = 4, 8, 12,$ and $16,$ respectively. For better visualization, we set the colors of the newly interpolated points as those of the nearest input points.

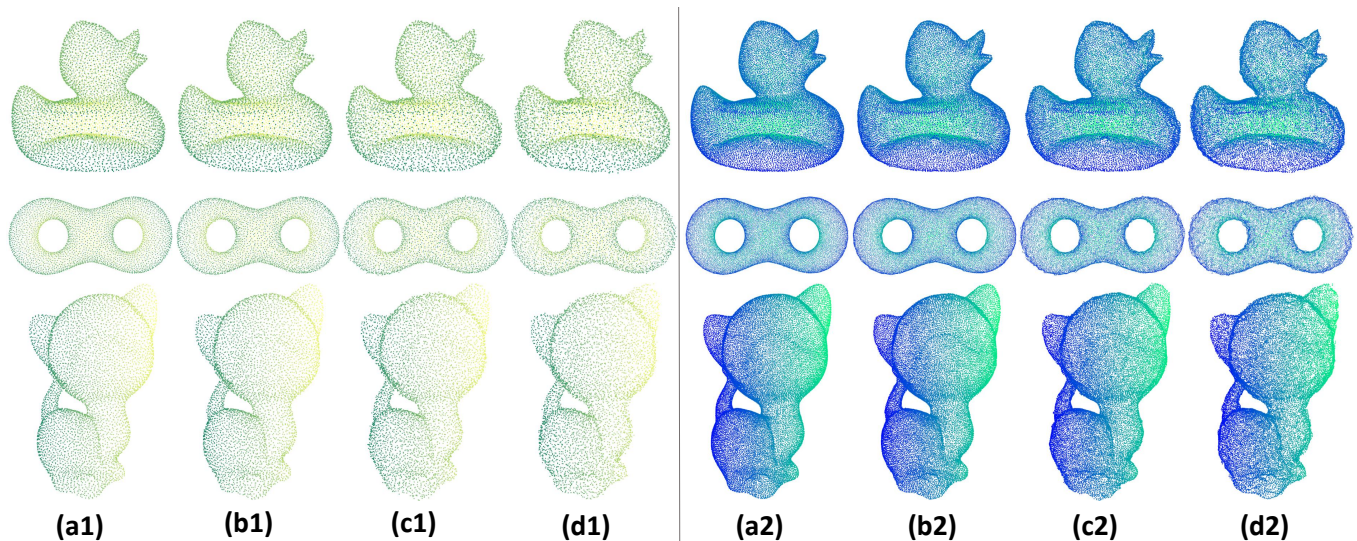


Fig. 9: Evaluation of MAPU-Net on noisy inputs. Left: (a1), (b1), (c1), and (d1) are the sparse inputs with 0%, 0.5%, 1.0%, and 1.5% Gaussian noise, respectively. Right: (a2), (b2), (c2), and (d2) are the $4\times$ upsampled results from (a1), (b1), (c1), and (d1), respectively.

pared with 3PU-Net and PU-GAN-G, the proposed MAPU-Net can recover sharper features and more accurate object shapes while introducing much fewer outliers, which may be beneficial to downstream applications, such as object classification/recognition. Fig. 8 shows more visual results of real world data upsampled by the proposed MAPU-Net. Here we also displayed the associated colors of the point clouds for better visualization purposes. Particularly, the color attributes of newly upsampled points are kept identical to the closest points in the sparse input. From Fig. 8, it can be seen that the quality of upsampled point clouds gradually improves with

the upsampling factor increasing, i.e., more geometry details exhibit.

Finally, we demonstrated the robustness of MAPU-Net on noisy inputs. Fig. 9 visualizes the upsampled results by MAPU-Net from various noisy point clouds, which have three levels of noise with the standard deviation equal to 0.5%, 1.0% and 1.5% of the bounding box diagonal. We observed that the results from the noisy inputs are close to those from noise-free inputs, demonstrating the robustness of MAPU-Net to noise.

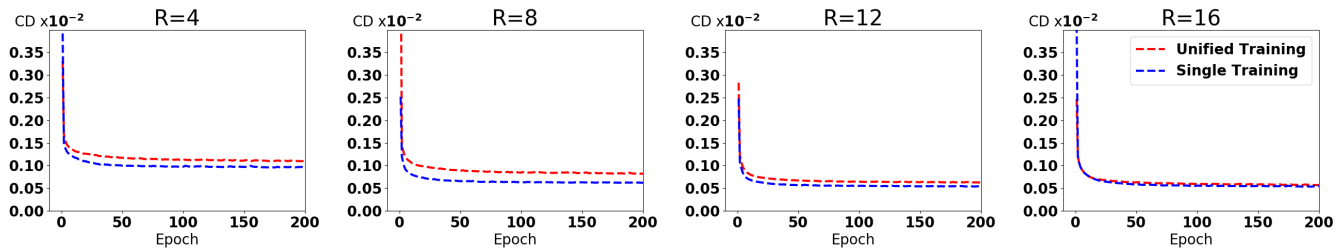


Fig. 10: Comparison of training losses of the proposed unified MAPU-Net and the MAPU-Net trained for a single upsampling factor. All the subfigures share the same legend.

D. Ablation Study

To deeply understand MAPU-Net, we studied the effectiveness of each module. As listed in Table II, the 1st and 2nd rows indicate that the distance encoder and the refinement module were removed from MAPU-Net, respectively, the 3rd row indicates that the refinement module was realized by directly learning offsets without the guidance of normals, and the 4th row indicates that there was no P2F loss when training MAPU-Net. It can be concluded that all modules make contributions because the performance degradation is caused when removing any module.

To investigate the efficiency and effectiveness of our strategy, we trained a unified MAPU-Net, denoted by *Unified-Training*, as well as multiple MAPU-Nets - each with a single and fixed upsampling factor - denoted by *Single-Training*. We then compared the training losses under the two types of settings. Here the loss refers to the patch-wise CD. As illustrated in Fig. 10, for an identical factor MAPU-Net converges to a comparable value under these two training settings, validating the effectiveness of our unified training strategy. Moreover, we observed that MAPU-Net has a similar convergence rate under the two training settings, i.e., the CD value reduces slightly after 25 epochs, which validates its efficiency. In other words, our unified training strategy does not consume additional computational resources.

VI. CONCLUSION

We presented MAPU-Net, a novel end-to-end learning framework for magnification-arbitrary point cloud upsampling. As a neural network built upon an explicit formulation of the upsampling problem using linear approximation, MAPU-Net is interpretable and compact. It distinguishes itself from the deep learning peers in flexibility: trained once a single network of MAPU-Net is able to generate dense point clouds for an arbitrary factor. Quantitative evaluation on synthetic data shows that MAPU-Net is more accurate and can produce richer and more meaningful geometric details than state-of-the-art methods. We also demonstrated the effectiveness and advantage of MAPU-Net on noisy data and real-world data. In the future, we will extend MAPU-Net to simultaneously increase the resolution of geometry and the associated attributes (e.g., colors) of point clouds. Moreover, we will investigate the potential of MAPU-Net in point cloud compression, which is highly demanded for efficient storage and transmission.

REFERENCES

- [1] Sketchfab. <https://sketchfab.com>.
- [2] P. Achlioptas, O. Diamanti, I. Mitliagkas, and L. Guibas. Learning representations and generative models for 3d point clouds. In *International conference on machine learning*, pages 40–49, 2018.
- [3] M. Alexa, J. Behr, D. Cohen-Or, S. Fleishman, D. Levin, and C. T. Silva. Computing and rendering point set surfaces. *IEEE Transactions on Visualization and Computer Graphics*, 9(1):3–15, 2003.
- [4] M. Bolognesi, A. Furini, V. Russo, A. Pellegrinelli, and P. Russo. Testing the low-cost rpaas potential in 3d cultural heritage reconstruction. *International Archives of the Photogrammetry, Remote Sensing & Spatial Information Sciences*, 2015.
- [5] X. Chen, H. Ma, J. Wan, B. Li, and T. Xia. Multi-view 3d object detection network for autonomous driving. In *Proceedings of the IEEE Conference on Computer Vision and Pattern Recognition*, pages 1907–1915, 2017.
- [6] M. Corsini, P. Cignoni, and R. Scopigno. Efficient and flexible sampling with blue noise properties of triangular meshes. *IEEE Transactions on Visualization and Computer Graphics*, 18(6):914–924, 2012.
- [7] H. Deng, T. Birdal, and S. Ilic. Ppf-foldnet: Unsupervised learning of rotation invariant 3d local descriptors. In *Proceedings of the European Conference on Computer Vision (ECCV)*, pages 602–618, 2018.
- [8] E. D’Eon, B. Harrison, T. Myers, and P. A. Chou. 8i voxelized full bodies—a voxelized point cloud dataset, document iso/iec jtc1/sc29 joint wg11/wg1 (mpeg/jpeg), wg11m40059/ wg1m74006. 2017.
- [9] Y. Eldar, M. Lindenbaum, M. Porat, and Y. Y. Zeevi. The farthest point strategy for progressive image sampling. *IEEE Transactions on Image Processing*, 6(9):1305–1315, 1997.
- [10] A. Geiger, P. Lenz, C. Stiller, and R. Urtasun. Vision meets robotics: The kitti dataset. *International Journal of Robotics Research (IJRR)*, 2013.
- [11] T. Hakala, J. Suomalainen, S. Kaasalainen, and Y. Chen. Full waveform hyperspectral lidar for terrestrial laser scanning. *Optics Express*, 20(7):7119–7127, 2012.
- [12] R. Held, A. Gupta, B. Curless, and M. Agrawala. 3d puppetry: a kinect-based interface for 3d animation. In *UIST*, pages 423–434. Citeseer, 2012.
- [13] F. B. Hildebrand. *Advanced calculus for applications*. 1962.
- [14] Q. Hu, B. Yang, L. Xie, S. Rosa, Y. Guo, Z. Wang, N. Trigoni, and A. Markham. Randla-net: Efficient semantic segmentation of large-scale point clouds. In *Proceedings of the IEEE/CVF Conference on Computer Vision and Pattern Recognition*, pages 11108–11117, 2020.
- [15] H. Huang, D. Li, H. Zhang, U. Ascher, and D. Cohen-Or. Consolidation of unorganized point clouds for surface reconstruction. *ACM Transactions on Graphics (TOG)*, 28(5):176, 2009.
- [16] H. Huang, S. Wu, M. Gong, D. Cohen-Or, U. Ascher, and H. R. Zhang. Edge-aware point set resampling. *ACM Transactions on Graphics (TOG)*, 32(1):9, 2013.
- [17] M. Kazhdan and H. Hoppe. Screened poisson surface reconstruction. *ACM Transactions on Graphics (ToG)*, 32(3):29, 2013.
- [18] K. Kimoto, N. Asada, T. Mori, Y. Hara, A. Ohya, et al. Development of small size 3d lidar. In *2014 IEEE International Conference on Robotics and Automation (ICRA)*, pages 4620–4626. IEEE, 2014.
- [19] D. P. Kingma and J. Ba. Adam: A method for stochastic optimization. *International Conference on Learning Representations (ICLR)*, 2015.
- [20] F. Lafarge and C. Mallet. Creating large-scale city models from 3d-point clouds: a robust approach with hybrid representation. *International Journal of Computer Vision*, 99(1):69–85, 2012.

- [21] W.-S. Lai, J.-B. Huang, N. Ahuja, and M.-H. Yang. Deep laplacian pyramid networks for fast and accurate super-resolution. In *Proceedings of the IEEE Conference on Computer Vision and Pattern Recognition*, pages 624–632, 2017.
- [22] B. Li. 3d fully convolutional network for vehicle detection in point cloud. In *2017 IEEE/RSJ International Conference on Intelligent Robots and Systems (IROS)*, pages 1513–1518. IEEE, 2017.
- [23] R. Li, X. Li, C.-W. Fu, D. Cohen-Or, and P.-A. Heng. Pu-gan: a point cloud upsampling adversarial network. In *Proceedings of the IEEE International Conference on Computer Vision*, pages 7203–7212, 2019.
- [24] Y. Li, R. Bu, M. Sun, W. Wu, X. Di, and B. Chen. Pointcnn: Convolution on x-transformed points. In *Advances in Neural Information Processing Systems*, pages 820–830, 2018.
- [25] Y. Lipman, D. Cohen-Or, D. Levin, and H. Tal-Ezer. Parameterization-free projection for geometry reconstruction. In *ACM Transactions on Graphics (TOG)*, volume 26, page 22. ACM, 2007.
- [26] W. Lu, G. Wan, Y. Zhou, X. Fu, P. Yuan, and S. Song. Deepvcp: An end-to-end deep neural network for point cloud registration. In *Proceedings of the IEEE International Conference on Computer Vision*, pages 12–21, 2019.
- [27] P. Musialski, P. Wonka, D. G. Aliaga, M. Wimmer, L. Van Gool, and W. Purgathofer. A survey of urban reconstruction. In *Computer Graphics Forum*, volume 32, pages 146–177. Wiley Online Library, 2013.
- [28] S. Nie, C. Wang, P. Dong, X. Xi, S. Luo, and H. Zhou. Estimating leaf area index of maize using airborne discrete-return lidar data. *IEEE Journal of Selected Topics in Applied Earth Observations and Remote Sensing*, 9(7):3259–3266, 2016.
- [29] S. Orts-Escolano, C. Rhemann, S. Fanello, W. Chang, A. Kowdle, Y. Degtyarev, D. Kim, P. L. Davidson, S. Khamis, M. Dou, et al. Holoportation: Virtual 3d teleportation in real-time. In *Proceedings of the 29th Annual Symposium on User Interface Software and Technology*, pages 741–754. ACM, 2016.
- [30] J. G. Paine, T. L. Caudle, and J. R. Andrews. Shoreline and sand storage dynamics from annual airborne lidar surveys, texas gulf coast. *Journal of Coastal Research*, 33(3):487–506, 2016.
- [31] R. Preiner, O. Mattausch, M. Arikani, R. Pajarola, and M. Wimmer. Continuous projection for fast I1 reconstruction. *ACM Transactions on Graphics (TOG)*, 33(4):47–1, 2014.
- [32] C. R. Qi, O. Litany, K. He, and L. J. Guibas. Deep hough voting for 3d object detection in point clouds. In *Proceedings of the IEEE International Conference on Computer Vision*, pages 9277–9286, 2019.
- [33] C. R. Qi, W. Liu, C. Wu, H. Su, and L. J. Guibas. Frustum pointnets for 3d object detection from rgb-d data. In *Proceedings of the IEEE conference on computer vision and pattern recognition*, pages 918–927, 2018.
- [34] C. R. Qi, H. Su, K. Mo, and L. J. Guibas. Pointnet: Deep learning on point sets for 3d classification and segmentation. In *Proceedings of the IEEE Conference on Computer Vision and Pattern Recognition*, pages 652–660, 2017.
- [35] C. R. Qi, L. Yi, H. Su, and L. J. Guibas. Pointnet++: Deep hierarchical feature learning on point sets in a metric space. In *Advances in Neural Information Processing Systems*, pages 5099–5108, 2017.
- [36] Y. Qian, J. Hou, S. Kwong, and Y. He. Pugeo-net: A geometry-centric network for 3d point cloud upsampling. *Proceedings of the European Conference on Computer Vision (ECCV)*, 2020.
- [37] J. M. Santana, J. Wendel, A. Trujillo, J. P. Suárez, A. Simons, and A. Koch. Multimodal location based services—semantic 3d city data as virtual and augmented reality. In *Progress in Location-based Services 2016*, pages 329–353. Springer, 2017.
- [38] S. Schwarz and D. Flynn. Common test conditions for point cloud compression. *ISO/IEC JTC1/SC29/WG11 MPEG, N19084*, 2020.
- [39] S. Shi, X. Wang, and H. Li. Pointcnn: 3d object proposal generation and detection from point cloud. In *Proceedings of the IEEE Conference on Computer Vision and Pattern Recognition*, pages 770–779, 2019.
- [40] Y. Wang and J. M. Solomon. Deep closest point: Learning representations for point cloud registration. In *Proceedings of the IEEE International Conference on Computer Vision*, pages 3523–3532, 2019.
- [41] Y. Wang, Y. Sun, Z. Liu, S. E. Sarma, M. M. Bronstein, and J. M. Solomon. Dynamic graph cnn for learning on point clouds. *ACM Transactions on Graphics (TOG)*, 38(5):146, 2019.
- [42] Y. Wang, S. Wu, H. Huang, D. Cohen-Or, and O. Sorkine-Hornung. Patch-based progressive 3d point set upsampling. In *Proceedings of the IEEE Conference on Computer Vision and Pattern Recognition*, pages 5958–5967, 2019.
- [43] S. Wu, H. Huang, M. Gong, M. Zwicker, and D. Cohen-Or. Deep points consolidation. *ACM Transactions on Graphics (ToG)*, 34(6):1–13, 2015.
- [44] Z. Xu, L. Wu, Y. Shen, F. Li, Q. Wang, and R. Wang. Tridimensional reconstruction applied to cultural heritage with the use of camera-equipped uav and terrestrial laser scanner. *Remote Sensing*, 6(11):10413–10434, 2014.
- [45] Y. Yang, C. Feng, Y. Shen, and D. Tian. Foldingnet: Point cloud auto-encoder via deep grid deformation. In *Proceedings of the IEEE Conference on Computer Vision and Pattern Recognition*, pages 206–215, 2018.
- [46] Z. J. Yew and G. H. Lee. 3dfeat-net: Weakly supervised local 3d features for point cloud registration. In *European Conference on Computer Vision*, pages 630–646. Springer, 2018.
- [47] L. Yu, X. Li, C.-W. Fu, D. Cohen-Or, and P.-A. Heng. Ec-net: an edge-aware point set consolidation network. In *Proceedings of the European Conference on Computer Vision (ECCV)*, pages 386–402, 2018.
- [48] L. Yu, X. Li, C.-W. Fu, D. Cohen-Or, and P.-A. Heng. Pu-net: Point cloud upsampling network. In *Proceedings of the IEEE Conference on Computer Vision and Pattern Recognition*, pages 2790–2799, 2018.
- [49] Y. Zhang, Y. Tian, Y. Kong, B. Zhong, and Y. Fu. Residual dense network for image super-resolution. In *Proceedings of the IEEE Conference on Computer Vision and Pattern Recognition*, pages 2472–2481, 2018.